Atmospheric Environment 214 (2019) 116880

Contents lists available at ScienceDirect

Atmospheric Environment

journal homepage: www.elsevier.com/locate/atmosenv

An examination of the algorithm for estimating light extinction from IMPROVE particle speciation data

A.J. Prenni[a,*], J.L. Hand[b], W.C. Malm[b], S. Copeland[b], G. Luo[c], F. Yu[c], N. Taylor[d], L.M. Russell[e], B.A. Schichtel[a]

[a] National Park Service, Air Resources Division, Lakewood, CO, USA
[b] Cooperative Institute for Research in the Atmosphere (CIRA), Colorado State University, Fort Collins, CO, USA
[c] Atmospheric Sciences Research Center, State University of New York at Albany, NY, USA
[d] Environmental Protection Agency, Washington, DC, USA
[e] Scripps Institution of Oceanography, University of California, San Diego, CA, USA

ARTICLE INFO

Keywords:
IMPROVE equation
Light scattering
Remote aerosols
$PM_{2.5}$ mass
Nephelometers

ABSTRACT

The Interagency Monitoring of Protected Visual Environments (IMPROVE) network is the basis for monitoring visibility in Class I Areas throughout the United States. Monitoring is conducted by collecting $PM_{2.5}$ and PM_{10} samples every third day at over 150 remote and rural sites nationwide, with $PM_{2.5}$ samples being analyzed for chemical composition. Light extinction is reconstructed using an algorithm that relates speciated mass to light extinction based on aerosol mass and size (second IMPROVE equation). In addition, the National Park Service directly measures light scattering at a subset of IMPROVE sites using Optec NGN-2 integrating nephelometers. The optical measurements serve as a check of the reconstructed scattering, in that measured scattering from the nephelometers and reconstructed scattering from the second IMPROVE equation should be equivalent. During its development, the second IMPROVE equation was shown to accurately estimate light scattering for a broad range of aerosol compositions and loadings for samples collected through 2003. Here reconstructed scattering is assessed from the second IMPROVE equation by comparing measured light scattering from nephelometers to reconstructed light scattering at 11 collocated sites over a 16 year period (2001–2016). The comparisons suggest that the relationship between measured and reconstructed light scattering has changed over time and that in recent years the second IMPROVE equation has underestimated light scattering at many sites. This shift toward poorer agreement corresponds to periods with relatively large decreases in sulfate and organic mass concentrations. These decreases lead to biases in reconstructed scattering calculated with the second IMPROVE equation, due to the assumed relationship between mass concentration and size distribution. This relationship, referred to as the split component algorithm, appears to be flawed as currently implemented. A potential approach is explored that scales the split component algorithm each year and at each site, based on measured mass concentrations at the site. The proposed approach appears to reduce the biases in the second IMPROVE equation.

1. Introduction

Degradation of visibility is among the most easily detectable effects of particulate air pollution in the atmosphere. Under the Clean Air Act, Congress recognized that visibility is a resource to be valued and set forth a national goal that calls for "the prevention of any future, and the remedying of any existing, impairment of visibility in mandatory Class I federal areas which impairment results from manmade air pollution" (42 U.S.C. § 7491). Class I Areas (CIAs) consist of international parks, national parks larger than 6000 acres, and wilderness areas and national memorial parks larger than 5000 acres that were in existence as of 7 August 1977. To safeguard visibility in these areas, federal land managers were assigned the "affirmative responsibility to protect the air quality related values (including visibility)" of Class I lands (42 U.S.C. § 7475). The Environmental Protection Agency's (EPA) Regional Haze Rule (RHR) expanded this responsibility by requiring monitoring in locations representative of the 156 visibility-protected CIAs (64 Fed. Reg. 35, 1999 714), and the IMPROVE (Interagency Monitoring of PROtected Visual Environments) program (Malm et al., 1994) was designated as the visibility monitoring network.

The purposes of the IMPROVE network are to establish current visibility conditions, to identify chemical species and emission sources

* Corresponding author.
E-mail address: anthony_prenni@nps.gov (A.J. Prenni).

https://doi.org/10.1016/j.atmosenv.2019.116880
Received 8 May 2019; Received in revised form 30 July 2019; Accepted 1 August 2019
Available online 02 August 2019
1352-2310/ Published by Elsevier Ltd.

responsible for existing anthropogenic visibility impairment (Gantt et al., 2018), and to document long-term trends for assessing progress toward the national visibility goal (Hand et al., 2011; Malm et al., 1994). IMPROVE modules collect $PM_{2.5}$ (particles less than 2.5 μm in diameter) and PM_{10} (particles less than 10 μm in diameter) samples, with the $PM_{2.5}$ samples being analyzed for chemical composition. Speciated aerosol data from IMPROVE are then used to calculate light extinction using the IMPROVE equation. The first IMPROVE equation determined light extinction based on Mie theory assuming a single aerosol size mode with a mass mean diameter of 0.4 μm, a geometric standard deviation of 2 (Malm et al., 1994), dry mass extinction efficiencies for sulfate, nitrate, organic mass, elemental carbon, soil and coarse mass, and humidity-dependent hygroscopic growth for sulfate and nitrate. Dry mass extinction efficiencies and hygroscopicities were based on literature values, and the aerosol was assumed to be externally mixed. A revised equation (second IMPROVE equation) was later introduced to reduce bias at the high and low light extinction regimes (Lowenthal and Kumar, 2003; Pitchford et al., 2007). The key revisions in the second IMPROVE equation include the addition of a sea salt term with associated hygroscopic growth, a change in the assumed organic compound mass (OM) to organic carbon (OC) mass ratio (OM/OC or Roc, from 1.4 to 1.8), the use of site-specific Rayleigh scattering, and the development of a split component extinction efficiency algorithm for ammonium sulfate, ammonium nitrate, and organic mass to model a bimodal size distribution. The second IMPROVE equation also includes light absorption for NO_2 for places where those data are available, but only aerosol species are considered here. The revised equation is:

$$b_{ext} = (2.2 \times f_s(RH) \times fAS_s + 4.8 \times f_L(RH) \times fAS_L) \times [Ammonium\ Sulfate] + (2.4 \times f_S(RH) \times fAN_s + 5.1 \times f_L(RH) \times fAN_L) \times [Ammonium\ Nitrate] + (2.8 \times fOMC_s + 6.1 \times fOMC_L) \times [Organic\ Mass] + 10 \times [Elemental\ Carbon] + 1 \times [Soil] + 1.7 \times f_{SS}(RH) \times [SS] + 0.6 \times [Coarse\ Mass] + Rayleigh\ Scattering\ (Site\ Specific) \quad (1)$$

Where light extinction (b_{ext}) and Rayleigh scattering are given in inverse megameters (Mm^{-1}); concentrations shown in brackets are in micrograms per meter cubed ($\mu g\ m^{-3}$); dry mass extinction efficiency terms, expressed as the prefactors for each component, are in meters squared per gram ($m^2\ g^{-1}$) and correspond to a wavelength ~550 nm; water growth terms, $f_S(RH)$ and $f_L(RH)$ for the small and large modes, respectively, are unitless; fAS_S and fAS_L are the mass fractions of ammonium sulfate in the small and large modes, respectively, with similar notation for ammonium nitrate (*fAN*) and organic mass (*fOMC*); and *SS* refers to sea salt. Values for the *f(RH)* terms can be found in Pitchford et al. (2007). The small and large modes of ammonium sulfate, ammonium nitrate, and organic mass are split based on their mass concentrations, with the assumption that lower concentrations are associated with fresher emissions and smaller particle sizes, while higher concentrations are associated with more aged and more processed aerosol and therefore larger sizes. This split component algorithm was developed because mass scattering efficiencies of ambient particles (e.g., (Malm et al., 2005)) and their individual components (see (Hand and Malm, 2007) and references therein) have been observed to vary, with the highest mass scattering efficiencies corresponding to periods with elevated fine mass concentrations (Hand and Malm, 2007; Lowenthal et al., 2009; Lowenthal and Kumar, 2004; Ryan et al., 2005; Tao et al., 2014). For this model, the mass scattering efficiencies of the small and large modes are based on Mie scattering calculations that assume lognormal size distributions with geometric mass mean diameters (D_g) and standard deviations (σ) of 0.2 μm (2.2) and 0.5 μm (1.5), respectively (Pitchford et al., 2007). For concentrations $\leq 20\ \mu g\ m^{-3}$, the fraction in the large mode is estimated by dividing the total concentration of the component by $20\ \mu g\ m^{-3}$. The remaining mass is in the small mode. This same factor of $20\ \mu g\ m^{-3}$ is used to apportion mass to different size modes for ammonium sulfate, ammonium nitrate, and organic mass, despite the relatively large differences in average mass of these species. For example, if the total fine particulate organic mass concentration is $5\ \mu g\ m^{-3}$, the fraction of organic aerosol in the large mode is calculated as $5\ \mu g\ m^{-3}/20\ \mu g\ m^{-3} = 1/4$ of $5\ \mu g\ m^{-3} = 1.25\ \mu g\ m^{-3}$; the remaining $3.75\ \mu g\ m^{-3}$ is in the small mode. If the total concentration of a component exceeds $20\ \mu g\ m^{-3}$, all of it is assumed to be in the large mode. A similar accounting is performed for ammonium sulfate and ammonium nitrate.

Equation (1) is based largely on literature values for light extinction and hygroscopic properties of the various aerosol components; however, the approach to splitting ammonium sulfate, ammonium nitrate, and organic mass into small and large modes was empirically derived. Previous analyses have found biases in the first (Lowenthal and Kumar, 2003; Malm and Hand, 2007) and second (Lowenthal et al., 2015) IMPROVE equations, both in terms of reconstructed mass and reconstructed extinction. Some of the potential issues with the second IMPROVE equation have been documented. For example, a constant Roc of 1.8 is used for all seasons and sites. However, organic aerosol can become more oxidized as it ages (Heald et al., 2010; Jimenez et al., 2009), and Roc has been shown to vary spatially (El-Zanan et al., 2005; Malm and Hand, 2007; Ruthenburg et al., 2014), seasonally (Malm and Hand, 2007; Malm et al., 2011; Polidori et al., 2008), and even during the course of a day (Aiken et al., 2008; Yu et al., 2005). As both anthropogenic and natural emissions of particles and aerosol precursors have changed over time (Blanchard et al., 2016; Hallar et al., 2017; Hidy et al., 2014; Malm et al., 2017; Prenni et al., 2016; Ridley et al., 2018), and will likely continue to change, the molecular form of carbonaceous aerosol will also likely be impacted. In addition, numerous studies have shown that ambient organic aerosol is often hygroscopic (Brock et al., 2016; Lowenthal et al., 2015; Prenni et al., 2007; Suda et al., 2014; Zhang et al., 2014, 2016), while organics are assumed to not be hygroscopic in both the first and second IMPROVE equations. Finally, all measured sulfate in the IMPROVE equation is assumed to be ammonium sulfate. However, data from around the United States indicate that sulfate is often not fully neutralized (Attwood et al., 2014; Hidy et al., 2014; Lee et al., 2008; Lowenthal et al., 2009, 2015; Malm and Day, 2001; Malm et al., 2003; Weber et al., 2016).

Given that a key function of IMPROVE monitoring is to track visibility progress at CIAs, Equation (1) must accurately model light extinction. As a check on calculated values, ambient light scattering is measured at a subset of IMPROVE sites. In this paper, reconstructed scattering at 11 IMPROVE sites is compared to measured scattering to evaluate the performance of the second IMPROVE equation over a time period when aerosol mass and composition have changed dramatically (Hand et al., 2014; Malm et al., 2017; McClure and Jaffe, 2018). The causes for differences between measured and reconstructed scattering are investigated, and a potential method for adjusting the second IMPROVE equation is explored.

2. Materials and methods

All data used in this analysis are available on the Federal Land Manager Environmental Database (FED; http://views.cira.colostate.edu/fed/). IMPROVE and nephelometer data from 2001 to 2016 were downloaded in November 2018. Only data with data flag V0 ("Valid value") were used from the nephelometer dataset; all valid values from the IMPROVE dataset were used (V0 – V7).

The IMPROVE particle monitor consists of four independent sampling modules that collect 24-h samples on filters every third day. Three modules (A, B, and C) collect only fine particles ($PM_{2.5}$), while the fourth (module D) collects both fine and coarse particles (PM_{10}). Data from all of the modules are used to calculate visibility metrics. Module A is equipped with a Teflon® filter that is analyzed for $PM_{2.5}$ gravimetric fine mass, elemental concentrations with X-ray fluorescence (Hyslop et al., 2015), and light absorption using a hybrid integrating plate and sphere (White et al., 2016). Module B is fitted with a Nylasorb filter and is analyzed for the anions sulfate, nitrate, nitrite, and chloride

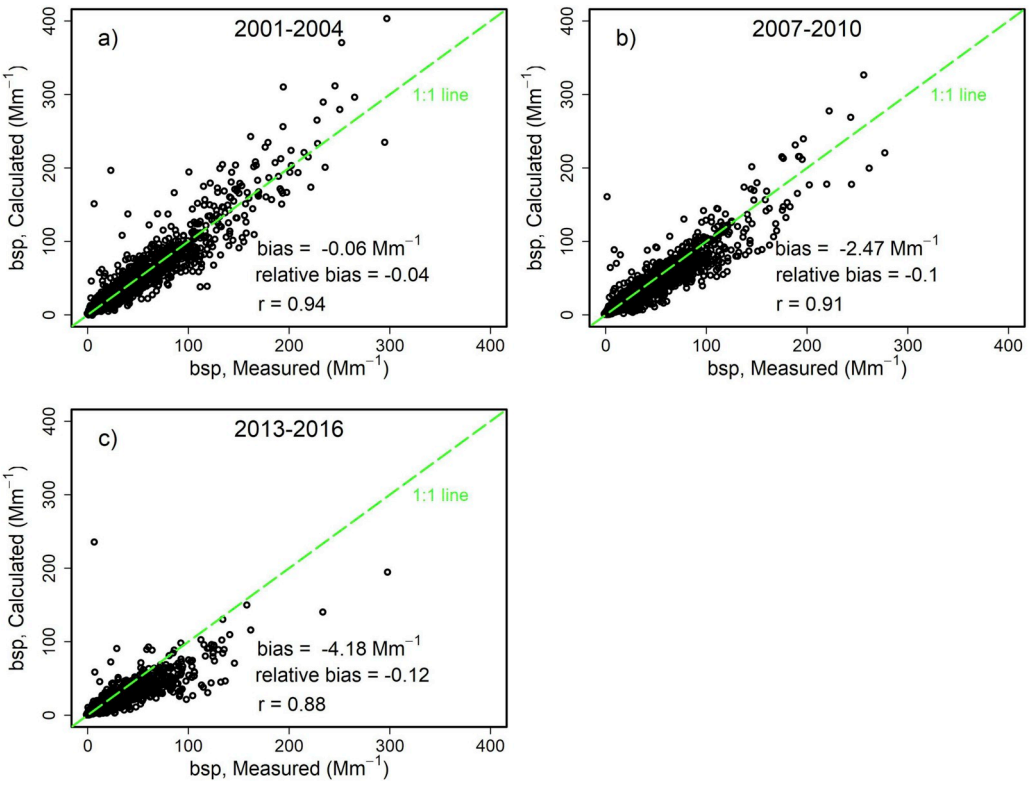

Fig. 1. Measured ambient aerosol scattering (bsp_{Meas}) versus calculated scattering (bsp_{Calc}). Data from all sites are used, as available. Data from three time periods are shown: (a) 2001–2004, (b) 2007–2010, and (c) 2013–2016. The bias (Mm^{-1}), relative bias, and Pearson correlation coefficient (r) for each time period are also shown, as wells as the 1:1 correspondence.

using ion chromatography. Module C uses a quartz fiber filter that is analyzed by thermal optical reflectance (TOR) for organic and elemental, or light absorbing, carbon (Chow et al., 2007). Module D is fitted with a PM_{10} inlet and utilizes a Teflon® filter to determine PM_{10} aerosol gravimetric mass. Coarse mass is determined as the difference between PM_{10} and $PM_{2.5}$ gravimetric mass. From Modules A-C, reconstructed fine mass (RCFM) can be calculated as:

RCFM = ammonium sulfate mass + ammonium nitrate mass + organic mass + elemental carbon mass + fine soil mass + sea salt mass (2)

Light scattering is measured at a subset of National Park Service (NPS) sites using Optec NGN-2 integrating nephelometers. Data from 11 nephelometers are used in this study; all are collocated with an IMPROVE sampler. Study sites include Acadia (ACAD; ME), Big Bend (BIBE; TX), Glacier (GLAC; MT), Great Basin (GRBA; NV) Grand Canyon (GRCA; AZ), Great Smoky Mountains (GRSM; TN), Mammoth Cave (MACA; KY), Mount Rainier (MORA; WA), National Capital (NACA, in Washington, D.C.; this site stopped operation in 2015), Rocky Mountain (ROMO; CO) and Shenandoah (SHEN; VA) National Parks. The Optec NGN-2 nephelometers use a unique integrating open air design (Optec NGN-2 Instrument Manual) to measure total ambient light scattering coefficients for all particle sizes in a known volume of air. The LED light source is centered at 530 nm with a bandwidth of 40 nm, which is then converted to an effective wavelength of 550 nm (Molenar and Persha, 2008). This air volume is illuminated by a near Lambertian diffuser. A telescope with a precisely defined field of view observes through a cylindrical pencil of air slightly above the diffuser, terminating in a light trap which reflects very little light back in the direction of the telescope. Measured light flux is proportional to light scattered by the sample plus light reflected from the surfaces in the optical chamber. Instruments are calibrated routinely using both zero air and span gas to convert the signal to particle light scattering. Because of the open air design, relative humidity (RH) and temperature of the air sample are essentially unchanged, so that the aerosol is negligibly modified when brought into the optical measuring chamber. Data are collected continuously and are reported as hourly averages. The primary upgrade to these instruments in recent years has been in changing from a lamp to an LED light source in 2011 (Molenar and Persha, 2008). Coarse particle scattering is underestimated when using the nephelometer due to a truncation error. This truncation error is highly variable and dependent on the size distribution. For a lognormal mass distribution with $D_g = 10\,\mu m$ and $\sigma_g = 1.75$, coarse mass scattering is underestimated by ~50%, while scattering corresponding to $D_g = 4\,\mu m$ is only underestimated by ~20% (Malm and Hand, 2007).

To compare measured light scattering from the nephelometer, bsp_{Meas}, and calculated scattering from the second IMPROVE equation, bsp_{Calc}, the contributions from elemental carbon absorption and Rayleigh scattering were removed from Equation (1), and the truncation error for coarse particles was accounted for by multiplying coarse scattering by 0.5. For the analysis below, nephelometer data were selected to match IMPROVE sample times, and nephelometer data have been filtered to only include measurements with RH < 90% and hourly values $bsp_{Meas} < 500\,Mm^{-1}$. For bsp_{Calc}, *f(RH)* values (Pitchford et al., 2007) were determined by calculating *f(RH)* for each hour and were averaged over the 24 h measurement period.

3. Results

3.1. Light scattering: measured versus reconstructed

The second IMPROVE equation was developed using data collected from 1995 through 2003, when aerosol concentrations across the country were generally higher than they are today (Hand et al., 2014; McClure and Jaffe, 2018) due to higher anthropogenic emissions. The composition of the aerosol has changed since this time due to relative changes in contributions from a variety of sources (e.g. (Attwood et al., 2014; Blanchard et al., 2013; Hand et al., 2012)) and related chemistry. bsp_{Calc} is compared to bsp_{meas} for all 11 sites for 2001 through 2016. Comparisons from 2001 to 2004, 2007 to 2010, and 2013 to 2016 are shown in Fig. 1a–c, respectively, including the biases and Pearson correlation coefficients for each of the three time periods. Bias is

calculated as $\Sigma(bsp_{Calc}\text{-}bsp_{Meas})/N$, where N is the number of observations; also shown in the figure are estimates of the relative bias, calculated as the median of $(bsp_{Calc}\text{-}bsp_{Meas})/bsp_{Meas}$ for all data points.

For the first time period shown (Fig. 1a), the measured and calculated scattering show close agreement (r = 0.94) with little bias; this likely results from the fact that the second IMPROVE equation was tuned to data that included this time period. However, over time, reconstructed light scattering has become underpredicted by the second IMPROVE equation, with the bias changing from $-0.06\,Mm^{-1}$ (relative bias = −0.04) for 2001–2004 data (Fig. 1a) to $-4.18\,Mm^{-1}$ (relative bias = −0.12) for 2013–2016 data (Fig. 1c). The bias for all data from 2001 to 2016 is $-2.59\,Mm^{-1}$ (relative bias = −0.09). Four of the sites (GLAC, GRBA, NACA, and ROMO) do not have data throughout the entire 2001–2016 time period. Limiting the comparison shown in Fig. 1 to sites that have data collection throughout 2001–2016 (ACAD, BIBE, GRCA, GRSM, MACA, MORA and SHEN) produces similar results (bias = $-2.70\,Mm^{-1}$; relative bias = −0.09).

To get a better understanding of the cause for this underprediction in recent years, Fig. 2 shows the annually averaged differences between bsp_{Calc} and bsp_{meas} from 2001 to 2016 for the five eastern parks, which have higher sulfate concentrations compared to the western parks (Hand et al., 2012), shown in Fig. 3. If the second IMPROVE equation accurately represented scattering, the average value of bsp_{Calc} - bsp_{meas} would be near zero, and would remain constant over time. Values greater than zero indicate that the second IMPROVE equation is overestimating scattering, while values less than zero suggest that the equation is underestimating scattering. Also shown are results from a Theil regression (Theil, 1950) (*TheilSen* function in R) on the daily values of this difference. A Theil regression was applied rather than an OLS regression to reduce the impact of outliers on the calculated slope. Annual average RCFM concentrations are also shown, along with annual average mass concentrations of ammonium sulfate, ammonium nitrate, and organics from IMPROVE. Several things are apparent from the figure. First, as has been shown previously (Attwood et al., 2014; Hand et al., 2014), $PM_{2.5}$ mass has decreased, in some cases dramatically, since 2001 at the five eastern sites. This trend has been driven largely by decreases in anthropogenic emissions of aerosol precursors (Hand et al., 2014; Sickles and Shadwick, 2015), leading to large decreases in sulfate and decreases in organic mass, which may be tied to the sulfate reductions (Malm et al., 2017; Xu et al., 2015). Similar decreases of aerosol precursors have been observed in parts of China (Zheng et al., 2018). Along with these declines, bsp_{Calc} has decreased at a faster rate than bsp_{meas}, resulting in a statistically significant ($p < 0.05$) decrease in their difference (bsp_{Calc} - bsp_{meas}) at all five of the eastern sites (trend lines in Fig. 2), indicating that the second IMPROVE equation is increasingly underestimating measured light scattering over time. The decrease does not correspond to a step function change at any time during the measurements, which might indicate a response to a change in measurement method, such as the switch to an LED light source in the nephelometers in 2011. Although the slopes are fairly small, over the 16 year period, this change can have a significant impact on calculated light extinction. For example, at GRSM, a slope of $-0.59\,Mm^{-1}\,yr^{-1}$ corresponds to a change of about $9\,Mm^{-1}$ during this time period; for comparison, the annual averaged bsp_{Meas} at GRSM for 2016 was $25\,Mm^{-1}$ (for measurements with RH < 90%). The underestimation of scattering from the second IMPROVE equation thus makes up a significant portion of extinction at the park. This artifact can lead to an overestimation of improvement in visibility at these parks when using IMPROVE data to calculate RHR metrics.

The trends in eastern parks can be compared to trends in western parks, where $PM_{2.5}$ mass concentrations are generally lower and where there have been less dramatic changes in $PM_{2.5}$ concentrations since 2001 (Fig. 3). In contrast to the eastern sites, only GLAC and MORA had statistically significant ($p < 0.05$) decreases in (bsp_{Calc} - bsp_{meas}) at the western sites (trend lines in Fig. 3). Note that GLAC can have significant impacts from wildfires, leading to elevated organic mass concentrations. BIBE and GRBA did not show statistically significant trends, and GRCA and ROMO had statistically significant ($p < 0.05$) increases in (bsp_{Calc} - bsp_{meas}). As a group, the western sites all have relatively low mass concentrations, and there is a much smaller change in concentrations, particularly for ammonium sulfate, over this time period.

3.2. Multiple linear regression

Throughout the United States, $PM_{2.5}$ mass and light extinction are often dominated by ammonium sulfate and organic mass (Hand et al., 2011), and so we focus on these aerosol components to try to better understand the differences and trends in Figs. 1–3. To this end, we employ multiple linear regression (MLR) to compare bsp_{meas} to the calculated scattering contributions of individual species. Equation (3) is a simplified version of the second IMPROVE equation (Equation (1)) aimed at determining whether scattering from individual species are being overestimated or underestimated:

$$bsp_{meas} = c_1 \times AS_{scat} + c_2 \times AN_{scat} + c_3 \times Organics_{scat} + c_4 \times Other_{scat} \quad (3)$$

For ammonium sulfate (AS_{scat}), ammonium nitrate (AN_{scat}) and organic mass ($Organics_{scat}$), all components of the second IMPROVE equation (Equation (1)) that contribute to scattering are included in each variable. For example, in Equation (3), $AS_{scat} = (2.2 \times f_s(RH) \times fAS_s + 4.8 \times f_L(RH) \times fAS_L) \times [Ammonium\ Sulfate]$; AN_{scat} and $Organics_{scat}$ are treated in the same manner. Despite the relatively low mass concentrations of ammonium nitrate, we include it in the regression analysis because it is one of the species for which the split component algorithm is applied. Soil, sea salt, and coarse mass contributions to scattering are combined into one variable ($Other_{scat}$). Regression coefficients greater than one indicate species and time periods for which calculated scattering is underestimated, and coefficients less than one indicate species and time periods for which calculated scattering is overestimated.

MLR results are shown in Figs. 4 and 5 for eastern and western parks, respectively. For all results, regressions were performed on a park by park basis, and results were averaged for each year for the eastern and western sites. Only regression coefficients with $p < 0.05$ from the regressions (*lm* function in R) were included. For ammonium nitrate, concentrations are typically low, except in winter, yielding noisy results at both eastern and western sites. The split component algorithm of the IMPROVE equation predicts that the majority of the ammonium nitrate mass is in the small mode due to these low concentrations; MLR results for ammonium nitrate will not be discussed further. The MLR results for the "Other" species are also noisy and are not shown in the figures. For eastern parks, a gradual increase in the MLR coefficient for ammonium sulfate is apparent after 2007. Such an increase suggests that the second IMPROVE equation is underpredicting contributions from ammonium sulfate beginning in 2008, and this bias is getting progressively larger. This trend corresponds to large decreases in ammonium sulfate concentrations at eastern sites during this same time period. Finally, the MLR coefficient for organic mass gradually increases over time, suggesting an underestimation of scattering from organic mass, consistent with observations that organic mass has been underpredicted in recent years (Hand et al., 2019), and again corresponding to a decrease in organic mass at these sites. The increasing trends in the ammonium sulfate and organic coefficients are both significant ($p < 0.01$) based on a Theil trend analysis of the annual coefficients (not shown, *TheilSen* function in R).

Results from western sites show important differences from eastern sites. For ammonium sulfate, there is a weaker increasing trend ($p < 0.1$) in the MLR coefficient; however, the average values are relatively high throughout the study period. Ammonium sulfate mass concentrations are lower at these western sites and do not show the

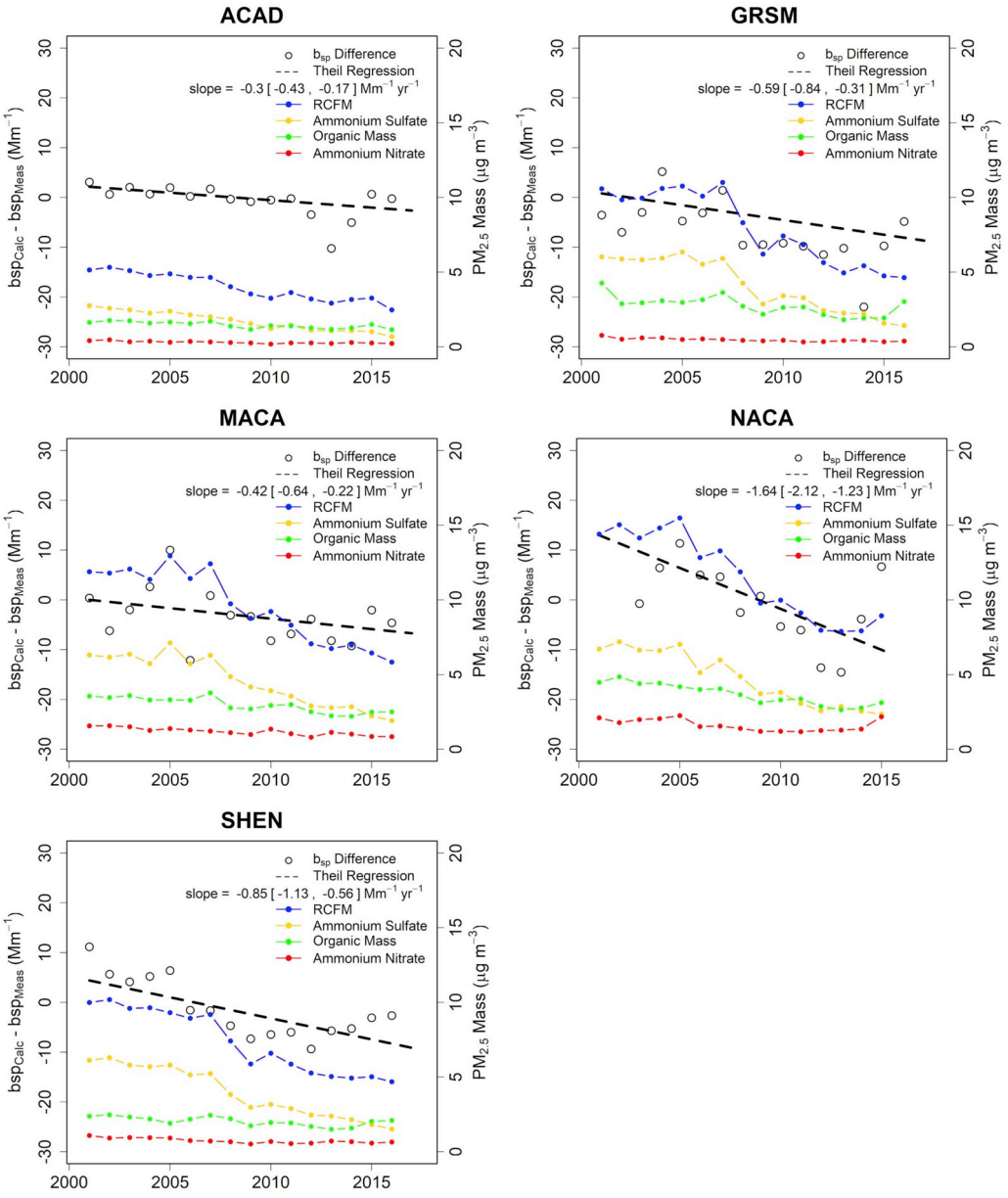

Fig. 2. Annually averaged differences between calculated scattering (bsp_{Calc}) and measured scattering (bsp_{Meas}) for eastern parks. Also shown are Theil regression trend lines using the daily data; for cases where the trends are significant, the 95% confidence intervals are included in brackets. On the right axis are annually averaged reconstructed fine mass (RCFM), ammonium sulfate, ammonium nitrate, and organic mass at each site (µg m^{-3}).

dramatic decreases over time as are seen at eastern parks. For organic mass, the MLR coefficients show a similar pattern as is observed in eastern parks, with coefficients showing a significant ($p < 0.01$) increasing trend, corresponding to decreases in organic mass. From Fig. 3, BIBE (ammonium sulfate) and GLAC (organic mass) stand out as having elevated concentrations in the west, relative to the other sites investigated. To determine whether the trends observed in Fig. 5 were driven primarily by these parks, regression coefficients were removed from the calculated mean values in Fig. 5 for both BIBE and GLAC. Although the average values of the coefficients did shift somewhat (not shown); the general trends remained unchanged, indicating that the trends in Fig. 5 are not driven exclusively by these two parks.

3.3. Mass scattering efficiencies

The trends shown in Figs. 4 and 5 likely result from a potential artifact in the second IMPROVE equation due to changes in the assumed physical characteristics of the aerosol as a function of aerosol composition and mass concentration since 2001. The split component algorithm of the second IMPROVE equation is directly impacted by changes in aerosol mass concentrations, allocating mass for ammonium sulfate, ammonium nitrate, and organics into small and large modes. Specifically, as concentrations of these species decrease, the split component algorithm moves an increasingly larger portion of the aerosol mass into the small mode. Because the dry mass scattering efficiency of the small mode is less than half that of the large mode, this presumed shift in size can have a large impact on calculated scattering. For example, Fig. 6 shows the average combined mass scattering efficiency for ammonium sulfate at GRSM and GRCA, which is determined by calculating the fractional contribution of the large and small modes, including the *f(RH)* terms (Equation (1)). The *f(RH)* terms are included here to ensure that any meteorological changes from this time period are included. As shown in the figure, there have been relatively large changes in the calculated ammonium sulfate mass scattering efficiency at GRSM, as

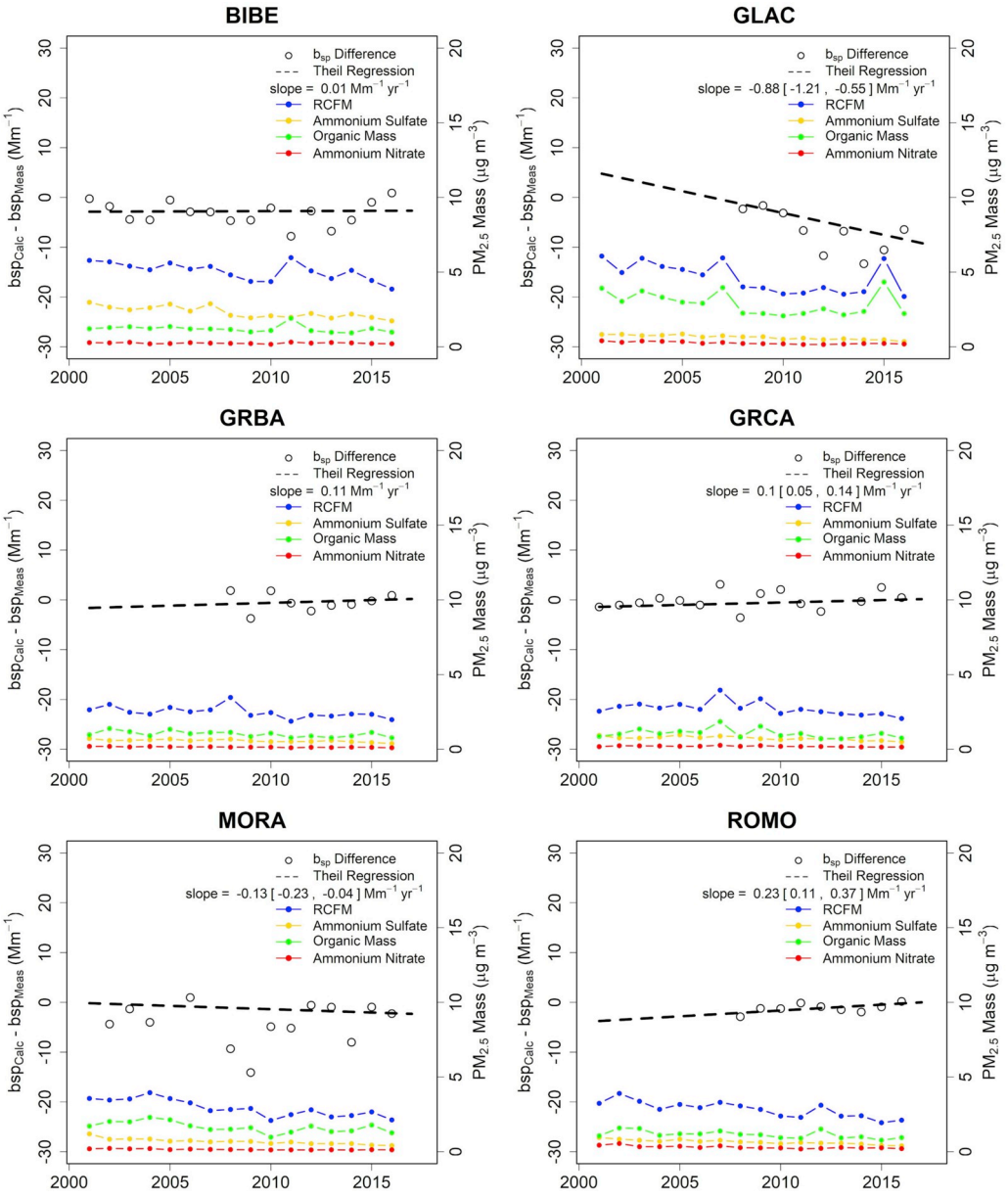

Fig. 3. Annually averaged differences between calculated scattering (bsp_{Calc}) and measured scattering (bsp_{Meas}) for western parks. Also shown are Theil regression trend lines using the daily data; for cases where the trends are significant, the 95% confidence intervals are included in brackets. On the right axis are annually averaged reconstructed fine mass (RCFM), ammonium sulfate, ammonium nitrate, and organic mass at each site (µg m^{-3}).

determined by the split component algorithm, where there have been large decreases in ammonium sulfate concentrations. However, there is little change in the calculated ammonium sulfate mass scattering efficiency at GRCA, where ammonium sulfate mass concentrations have been more stable. Also shown in Fig. 6 are annually averaged RH values from the two sites; the change in scattering efficiency at GRSM does not appear to be driven by RH. The large shift in scattering efficiency at GRSM, due to the split component algorithm of the second IMPROVE equation, is likely not representative of actual changes in mass scattering in the atmosphere.

The potential artifact in calculated mass scattering efficiencies at GRSM may also impact other sites across the network. Changes to the calculated average ambient scattering efficiencies of each species can be determined based on changes to aerosol mass at all IMPROVE sites. However, RH is not measured at all IMPROVE sites, and so only average dry mass scattering efficiencies are determined in the following discussion. For example, for ammonium sulfate the average combined dry mass scattering efficiency based on the split component algorithm is computed simply as $2.2 \times fAS_s + 4.8 \times fAS_l$. Similar calculations were carried out for ammonium nitrate and organic mass for all IMPROVE sites from 2001 to 2016. Trends in these calculated average dry mass scattering efficiencies are shown in Fig. 7a–c for all IMPROVE sites for ammonium sulfate, ammonium nitrate, and organic mass, respectively. Also shown in Fig. 7d are trends in reconstructed light extinction based on RHR annual mean values (http://views.cira.colostate.edu/fed/) and the second IMPROVE equation. In the figure, triangles represent IMPROVE sites. Downward-pointing triangles indicate decreasing trends, and upward-pointing triangles represent increasing trends, with filled symbols considered significant ($p < 0.10$). As shown in the figure, as aerosol concentrations have decreased throughout the United States, total reconstructed extinction and calculated average dry mass scattering efficiencies for all three species have also gone down. While reconstructed scattering is expected to decrease with decreasing aerosol concentrations, part of the observed trends are the result of the assumed

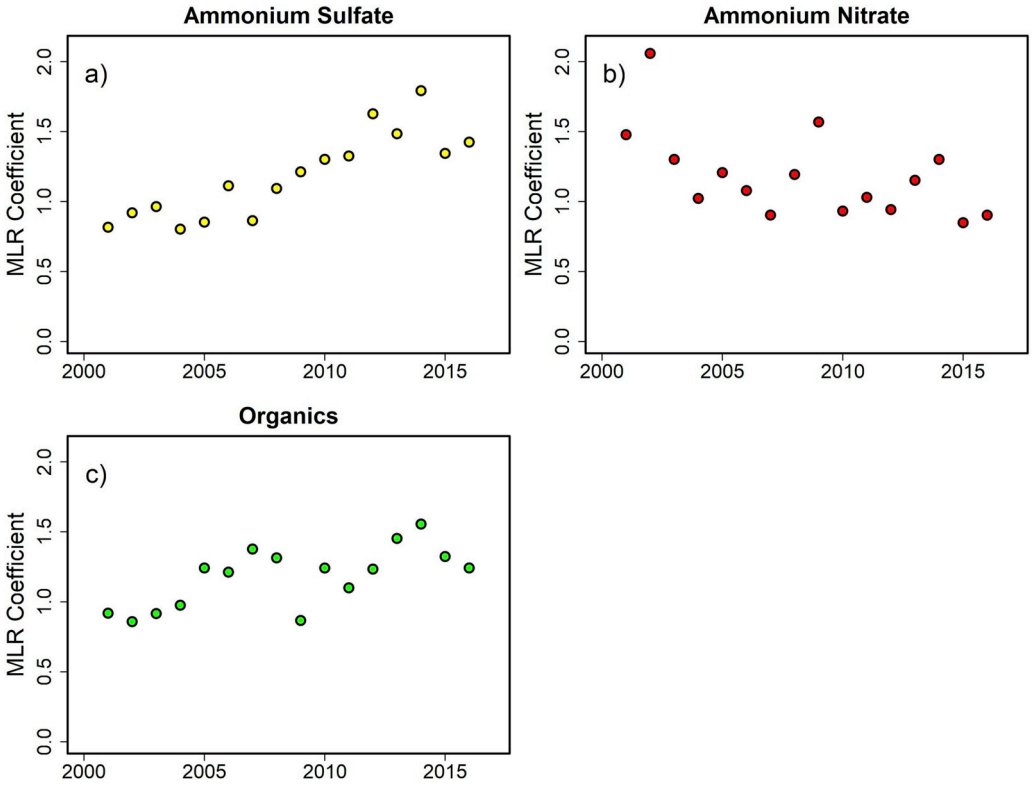

Fig. 4. Annual mean MLR coefficients from 2001 to 2016 using Equation (3) for eastern sites for (a) ammonium sulfate, (b) ammonium nitrate, and (c) organic mass.

changes in mass scattering efficiencies, which may not be occurring in the atmosphere. The decreases in scattering efficiencies of these species are likely, to some extent, artifacts due to the split component algorithm of the second IMPROVE equation. This is particularly true for ammonium sulfate in the east, where ammonium sulfate concentrations have decreased dramatically and where the greatest decreases in haze have been observed. The large decreases in calculated mass scattering efficiencies impact total extinction, and so we next assess whether these

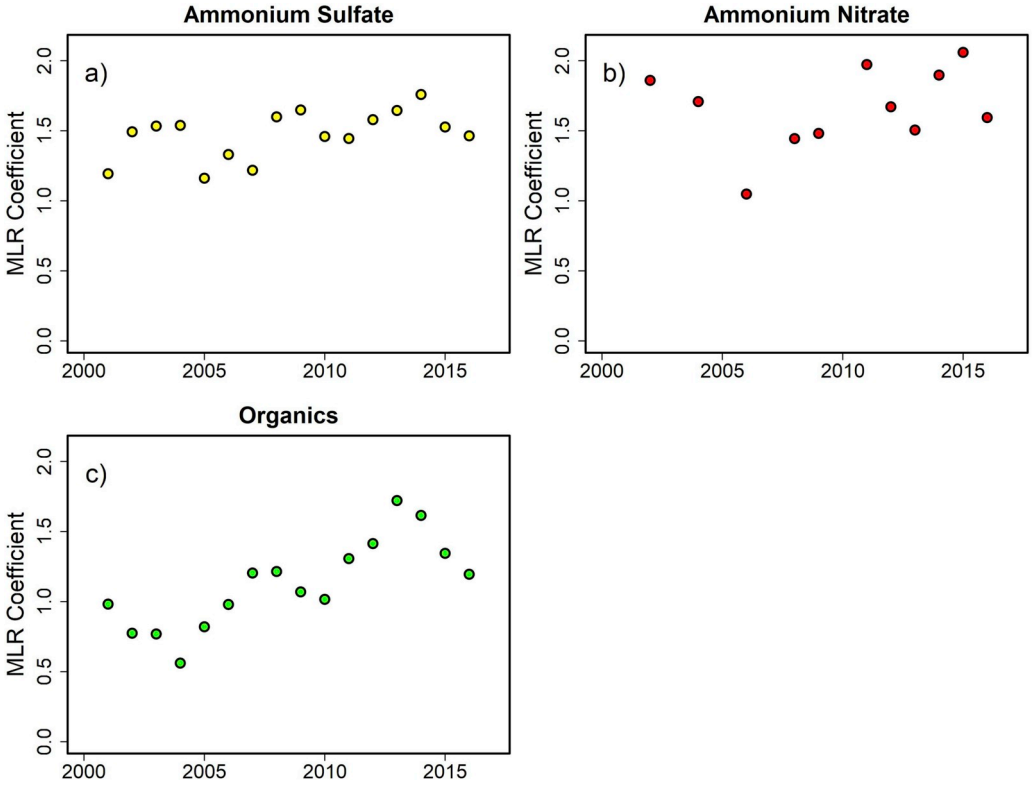

Fig. 5. Annual mean MLR coefficients from 2001 to 2016 using Equation (3) for western sites for (a) ammonium sulfate, (b) ammonium nitrate, and (c) organic mass.

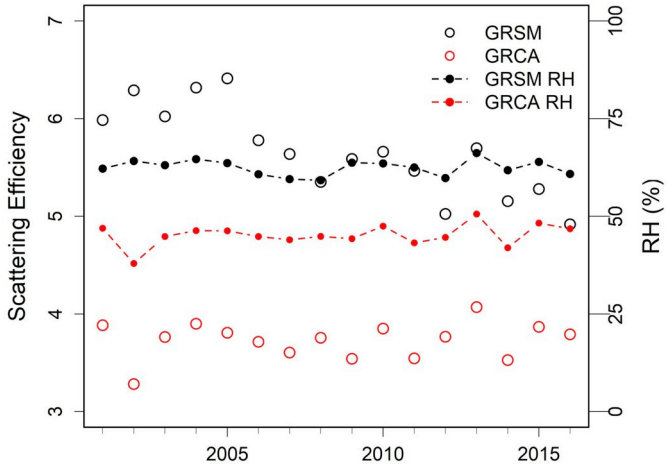

Fig. 6. Annually averaged ambient mass scattering efficiency ($m^2\ g^{-1}$) for ammonium sulfate, including the *f(RH)* term, at GRSM and GRCA, as determined from the second IMPROVE equation. Also shown are the annual average RH values for each site.

changes in calculated scattering efficiencies are representative of what is occurring in the atmosphere or are simply an artifact of the split component algorithm.

3.4. Measured size distributions at GRSM

Although the split component algorithm in the second IMPROVE equation is based on two aerosol size modes, aerosol size is not explicitly measured as part of IMPROVE. Size distribution data are available, however, for limited time periods as part of special studies conducted at some parks. Here we focus on three such studies from GRSM. The first set of measurements came from the Southeastern Aerosol and Visibility Study (SEAVS) (Hand et al., 2002) in July and August 1995. Several methods were used to collect aerosol size data (Hand et al., 2002), but we focus on dry (RH < 40%) size distributions measured using optical methods (Hand et al., 2000). Data from the second study come from Lowenthal et al. (2009, 2015). In this study, dry (RH < 20%) particle size distributions were measured with a scanning differential mobility analyzer. This study was conducted specifically to address questions related to the second IMPROVE equation. The third dataset comes from the Southern Oxidant and Aerosol Study (SOAS). Dry (RH < 50%) aerosol size distributions were measured by a scanning electrical mobility spectrometer (SEMS, Model, 2000C, Brechtel Manufacturing Incorporated) from 1 June 2013 to 18 July 2013 (Liu et al., 2017, 2018). Instruments were housed in a temperature-controlled container, and ambient air was pulled isokinetically through a 5 m inlet at about 900 L min^{-1} using a blower to provide sufficient bypass air to keep flow conditions constant (Bates et al., 2012).

The size distribution data from these three studies covered different ranges: SEAVS (122 nm–3 μm), 2006–2008 data (12–750 nm), and SOAS (10–896 nm). To compare the measurements, data were limited to a common size range (122 nm–750 nm), and single-mode, lognormal size distributions were fit to dry aerosol volume data for truncated distributions using *fitdist* in R. Although in some cases multiple modes were observed in the data, this approach was simply meant to approximate long-term trends in aerosol size. The fitted volume median diameters were then averaged for each day; results are shown in Fig. 8. Also shown are the average RCFM concentrations from IMPROVE for the corresponding time periods. Although the data were collected over an 18 year time period, they are shown by month. As shown in the figure and in Fig. 2, RCFM decreased significantly over this time period, driven largely by decreases in ammonium sulfate. Based on the split component algorithm of the second IMPROVE equation, such a decrease in mass should have shifted much of the aerosol mass from the large mode (D_{gv} = 0.5 μm; σ = 1.5) during SEAVS (for ammonium sulfate: large mode = 58%; small mode = 42%) to the small mode (D_{gv} = 0.2 μm; σ = 2.2) during SOAS (for ammonium sulfate: large mode = 13%; small mode = 87%). Such a shift in diameter was not observed nor was a change in σ (not shown). Instead, the largest sizes

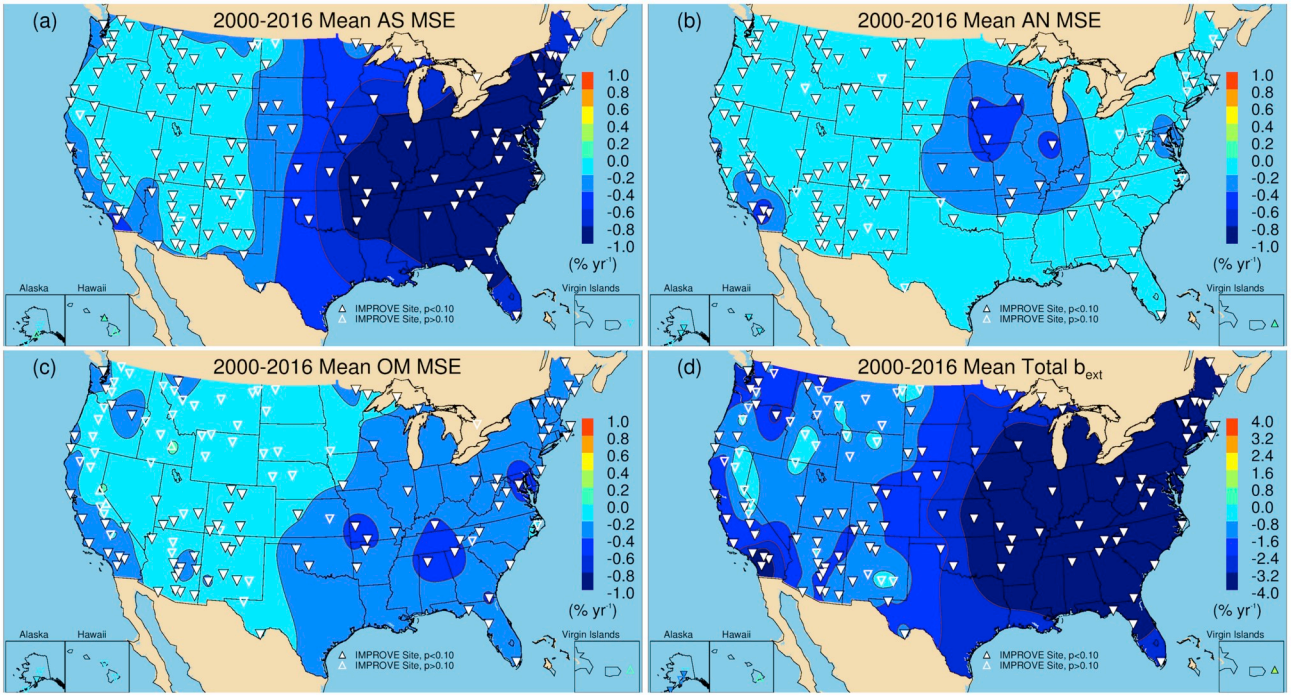

Fig. 7. IMPROVE 2001–2016 annual mean trends (% yr^{-1}) in (a) ammonium sulfate (AS), (b) ammonium nitrate (AN), and (c) organic mass (OM) average dry ambient mass scattering efficiencies (MSE), and (d) RHR total reconstructed light extinction (b_{ext}) across the United States. MSEs are determined based on the split component portion of the IMPROVE equation for each species.

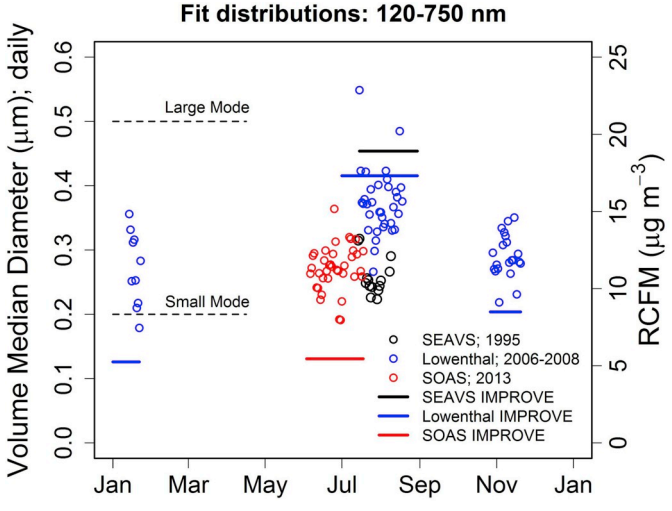

Fig. 8. Daily average dry volume median diameters at GRSM determined from single-mode, log-normal fits to the size distribution data (circles). Also shown are IMPROVE study average reconstructed fine mass values (µg m^{-3}) as solid lines for the overlapping time periods (right axis). The dashed lines show the mass mean diameter for the small and large modes in the second IMPROVE equation split component algorithm.

were observed during the summer of 2006 (Lowenthal et al., 2009), when aerosol concentrations were relatively high but still lower than observed during SEAVS. During this period, the split component algorithm would have predicted 57% in the large mode and 43% in the small mode for ammonium sulfate. In all studies, the dry volume median diameter generally fell between the predicted small and large modes from the second IMPROVE equation, as has been observed previously (Lowenthal et al., 2015). Based on these limited data, size distributions do not appear to be dependent on long-term trends in aerosol mass, indicating that the size dependence on mass in the second IMPROVE equation is no longer appropriate and is at least partially responsible for the biases in Figs. 1–3.

3.5. Modeled size distributions at GRSM

The limited datasets at GRSM are supported by recent modeling efforts based on the GEOS-Chem model (e.g. (Bey et al., 2001),) coupled with the size-resolved (sectional) Advanced Particle Microphysics (APM) package (Yu and Luo, 2009). The APM package, developed for implementation into global chemistry transport models and other weather and climate model systems (Luo and Yu, 2011b; Yu and Luo, 2009), explicitly simulates the evolution of particle size distributions in the atmosphere. A number of model-predicted particle properties have been evaluated against measurements, including mass concentration (Luo et al., 2019), number concentration (Luo and Yu, 2011a; Yu and Luo, 2009), optical properties (Yu et al., 2012), and size distributions (Yu et al., 2015). The long-term GEOS-Chem-APM simulation (2000–2016) was driven by the National Aeronautics and Space Administration's (NASA) Modern-Era Retrospective analysis for Research and Applications, Version 2 (MERRA-2). Global emissions for anthropogenic and natural sources are produced via the Harvard-NASA Emission Component version 1.0 (HEMCO) (Keller et al., 2014). Anthropogenic emissions over the United States are replaced with the EPA's National Emissions Inventory (NEI) Data. Air Pollutant Emissions Trends Data reported by the EPA are used to scale NEI 2011 emission inventories from year 2011 to the simulation year. New particle formation, an important process controlling particle size distributions, is calculated with the recently developed ternary ion-mediated nucleation of H_2SO_4–H_2O–NH_3 (Yu et al., 2018).

The modeled monthly average aerosol volume median diameter

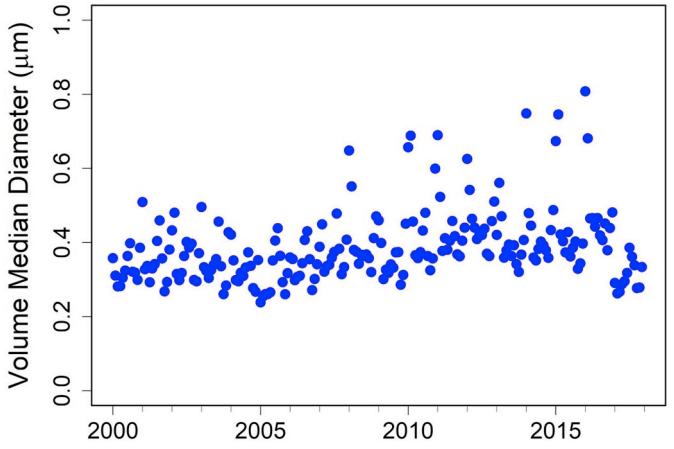

Fig. 9. Calculated volume median diameter (µm) at GRSM determined using an advanced particle microphysics (APM) model incorporated into a global chemistry transport model (GEOS-Chem). Results are for a grid cell centered at 36 °N and 85 °W.

(µm) in the 2° x 2.5° grid box containing GRSM (Fig. 9) is shown in Fig. 9 from 2000 to 2017. Volume median diameters are calculated from GEOS-Chem APM-simulated particle size distributions; they are representative of regional means near GRSM but are not specific to the park. Consistent with IMPROVE measured mass concentrations, the GEOS-CHEM model indicates a decline in $PM_{2.5}$ mass at GRSM (not shown). However, as shown in the figure, the results do not support a decrease in aerosol diameter during the study period. These results are consistent with the limited size distribution measurements shown above and are in contrast to the change in size suggested by the split component algorithm in the second IMPROVE equation.

4. Potential alternative approach

To better capture the dependence of light scattering on aerosol mass, we explore an alternative to the split component algorithm. The change is in how ammonium sulfate, ammonium nitrate, and organic mass are separated into the small and large modes. Rather than using a factor of 20 µg m^{-3} in the denominator of the split component algorithm, this factor is replaced each year by five times the annual median mass of each component at each site. Similar to the factor of 20 µg m^{-3} at the time it was implemented, five times the median represents the upper end of the observed mass distributions. A multiple of the median is used instead of an upper percentile of the distribution (e.g. 95th or 99th percentile) because it eliminates the extreme values that can occur in the measured distributions due to events such as wildfires. With this approach, the factor of 20 µg m^{-3} is replaced separately for ammonium sulfate, ammonium nitrate, and organic mass for each site each year. Typically, ammonium sulfate concentrations are highest in the east, organic mass concentrations are highest in the west (dependent on fires and seasonally dependent), ammonium nitrate concentrations are relatively lower at all eleven sites, and concentrations of all species have generally decreased over time, such that a range of factors may be used, even at a single site. This alternative approach attempts to correct for the biases shown in Fig. 1 while retaining the overall form of the second IMPROVE equation. Site-specific dry mass scattering efficiencies also have been explored at an urban site (Valentini et al., 2018) to attempt to improve scattering estimates.

Changing only this portion of the algorithm, bsp_{Calc} was recalculated and plotted against measured scattering, as shown in Fig. 10a–c for the three time periods. As is apparent in the figure, this approach shows reduced biases, although similar correlation coefficients, over the second IMPROVE equation (Fig. 1), particularly in later years (see Figs. 1c and 10c). When considering the entire time period

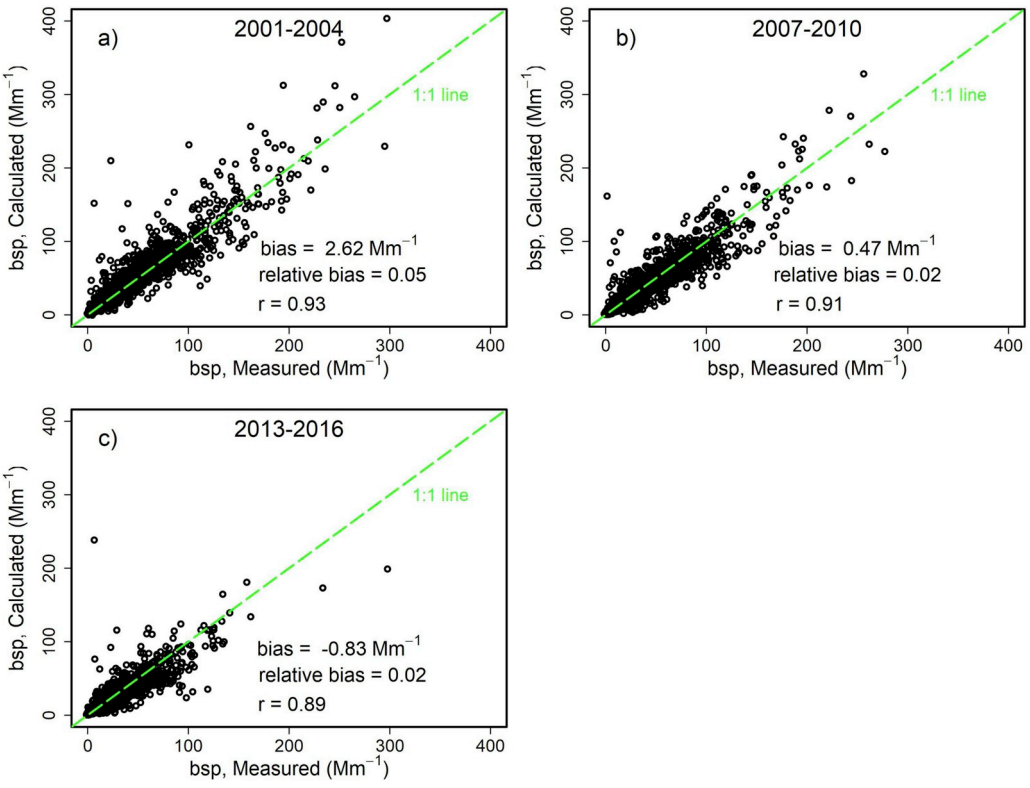

Fig. 10. Measured ambient aerosol scattering (bsp_{Meas}) versus calculated scattering (bsp_{Calc}), based on a revised version of the second IMPROVE equation for (a) 2001–2004; (b) 2007–2010; and (c) 2013–2016. Data from all 11 sites are used. The bias (Mm^{-1}), relative bias, and Pearson correlation coefficient (r) for each time period are also shown, as wells as the 1:1 correspondence.

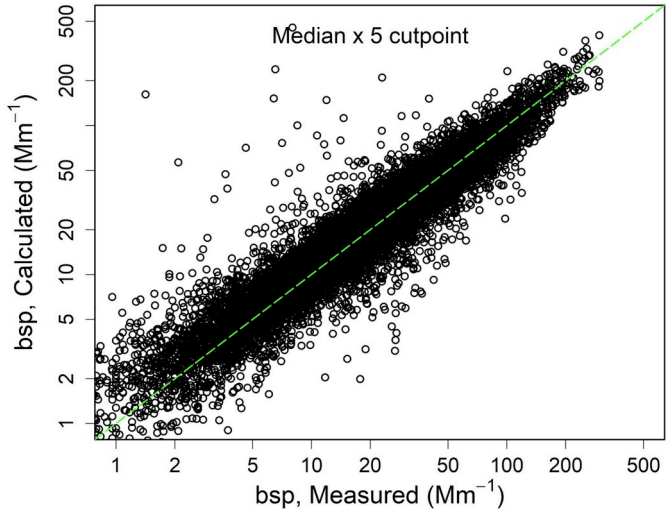

Fig. 11. Measured ambient aerosol scattering (bsp_{Meas}) versus calculated scattering (bsp_{Calc}), on a log-log scale, based on a revised version of the second IMPROVE equation for all sites from 2001 to 2016.

(2001–2016), this approach has a bias of 0.44 Mm^{-1} and a relative bias of 0.03, and the temporal trend in the biases are smaller than shown in Fig. 1. Fig. 11 shows data for all years across all sites on a log-log scale using this approach. The figure suggests reasonable agreement between measured and calculated scattering across the full range of scattering observed during the entire study period. The improvement indicates that such an approach may result in reconstructed scattering that more accurately reflects changes to visibility over time.

5. Conclusions

The split component algorithm of the second IMPROVE equation was intended to capture the relationship between light scattering and aerosol mass concentrations. This algorithm initially helped reduce bias in reconstructed scattering (Pitchford et al., 2007) for aerosol concentrations that were significantly higher than those observed today. However, the ability to accurately reconstruct ambient aerosol scattering has degraded over time, and the second IMPROVE equation currently underpredicts reconstructed light scattering at many IMPROVE sites. Specifically, the split component algorithm allocates too much aerosol mass into the small size mode, which has a lower dry mass scattering efficiency, leading to a persistent underestimation of light scattering in recent years. Underestimating light extinction using the second IMPROVE equation has major implications for implementation of the RHR, in that progress toward RHR goals is likely overestimated, especially in the east.

An alternative approach to the split component algorithm was explored. Rather than using one mass value to split all aerosol species into small and large aerosol size modes, ammonium sulfate, ammonium nitrate and organic mass were separated based on annual, site- and species-specific masses. This alternate approach appeared to reduce the biases in the reconstructed light scattering, and provide a promising framework for correcting the IMPROVE equation. However, recent analyses suggest that other assumptions in the IMPROVE mass reconstruction algorithm (Hand et al., 2019) may lead to biases that also likely impact reconstructed extinction. Potential biases with the reconstructed mass algorithm first must be understood and corrected before any changes to the second IMPROVE equation are proposed. There are potentially real chemical changes in the atmosphere that also may affect the assumptions made within the algorithm, such as a spatially and temporally variable Roc, a changing level of neutralization of sulfate, and changes to the hygroscopicity of organic aerosols, none of which are accounted for in the second IMPROVE equation. While it is nearly impossible to account for the impacts of changing atmospheric composition on aerosol extinction across the United States using a simple algorithm, any changes to the second IMPROVE equation will ideally account for the potential biases and will accurately represent visibility across the network.

Declaration of competing interest

☒ The authors declare that they have no known competing financial interests or personal relationships that could have appeared to influence the work reported in this paper.

Acknowledgments

The assumptions, findings, conclusions, judgments, and views presented herein are those of the authors and should not be interpreted as necessarily representing the National Park Service. G.L. and F.Y. acknowledge funding support from NASA under grant NNX13AK20G and the NSF under grant AGS1550816. Measurements by L.M.R. were supported by U.S. Environmental Protection Agency (EPA) grant RD-83540801. The EPA, through its Office of Research and Development, collaborated in the measurements during the SOAS campaign. The EPA does not endorse any products or commercial services mentioned in this publication. SOAS measurements used in this study are curated at http://doi.org/10.6075/J0P26W1T; SOAS measurements are also available at the project archive http://esrl.noaa.gov/csd/groups/csd7/measurements/2013senex/Ground/DataDownload.

Appendix A. Supplementary data

Supplementary data to this article can be found online at https://doi.org/10.1016/j.atmosenv.2019.116880.

References

Aiken, A.C., Decarlo, P.F., Kroll, J.H., Worsnop, D.R., Huffman, J.A., Docherty, K.S., Ulbrich, I.M., Mohr, C., Kimmel, J.R., Sueper, D., Sun, Y., Zhang, Q., Trimborn, A., Northway, M., Ziemann, P.J., Canagaratna, M.R., Onasch, T.B., Alfarra, M.R., Prevot, A.S.H., Dommen, J., Duplissy, J., Metzger, A., Baltensperger, U., Jimenez, J.L., 2008. O/C and OM/OC ratios of primary, secondary, and ambient organic aerosols with high-resolution time-of-flight aerosol mass spectrometry. Environ. Sci. Technol. 42, 4478–4485.

Attwood, A.R., Washenfelder, R.A., Brock, C.A., Hu, W., Baumann, K., Campuzano-Jost, P., Day, D.A., Edgerton, E.S., Murphy, D.M., Palm, B.B., McComiskey, A., Wagner, N.L., de Sa, S.S., Ortega, A., Martin, S.T., Jimenez, J.L., Brown, S.S., 2014. Trends in sulfate and organic aerosol mass in the Southeast U.S.: impact on aerosol optical depth and radiative forcing. Geophys. Res. Lett. 41, 7701–7709.

Bates, T.S., Quinn, P.K., Frossard, A.A., Russell, L.M., Hakala, J., Petaja, T., Kulmala, M., Covert, D.S., Cappa, C.D., Li, S.M., Hayden, K.L., Nuaaman, I., McLaren, R., Massoli, P., Canagaratna, M.R., Onasch, T.B., Sueper, D., Worsnop, D.R., Keene, W.C., 2012. Measurements of ocean derived aerosol off the coast of California. Journal of Geophysical Research-Atmospheres 117.

Bey, I., Jacob, D.J., Yantosca, R.M., Logan, J.A., Field, B.D., Fiore, A.M., Li, Q.B., Liu, H.G.Y., Mickley, L.J., Schultz, M.G., 2001. Global modeling of tropospheric chemistry with assimilated meteorology: model description and evaluation. Journal of Geophysical Research-Atmospheres 106, 23073–23095.

Blanchard, C.L., Hidy, G.M., Tanenbaum, S., Edgerton, E.S., Hartsell, B.E., 2013. The Southeastern Aerosol Research and Characterization (SEARCH) study: temporal trends in gas and PM concentrations and composition, 1999-2010. J. Air Waste Manag. Assoc. 63, 247–259.

Blanchard, C.L., Hidy, G.M., Shaw, S., Baumann, K., Edgerton, E.S., 2016. Effects of emission reductions on organic aerosol in the southeastern United States. Atmos. Chem. Phys. 16, 215–238.

Brock, C.A., Wagner, N.L., Anderson, B.E., Attwood, A.R., Beyersdorf, A., Campuzano-Jost, P., Carlton, A.G., Day, D.A., Diskin, G.S., Gordon, T.D., Jimenez, J.L., Lack, D.A., Liao, J., Markovic, M.Z., Middlebrook, A.M., Ng, N.L., Perring, A.E., Richardson, M.S., Schwarz, J.P., Washenfelder, R.A., Welti, A., Xu, L., Ziemba, L.D., Murphy, D.M., 2016. Aerosol optical properties in the southeastern United States in summer - Part 1: hygroscopic growth. Atmos. Chem. Phys. 16, 4987–5007.

Chow, J.C., Watson, J.G., Chen, L.W.A., Chang, M.C.O., Robinson, N.F., Trimble, D., Kohl, S., 2007. The IMPROVE-A temperature protocol for thermal/optical carbon analysis: maintaining consistency with a long-term database. J. Air Waste Manag. Assoc. 57, 1014–1023.

El-Zanan, H.S., Lowenthal, D.H., Zielinska, B., Chow, J.C., Kumar, N., 2005. Determination of the organic aerosol mass to organic carbon ratio in IMPROVE samples. Chemosphere 60, 485–496.

Fed Reg 35,714, July 1, 1999. Regional Haze Regulations, Codified at 40 CFR §§, vol. 51. pp. 300–309.

Gantt, B., Beaver, M., Timin, B., Lorang, P., 2018. Recommended metric for tracking visibility progress in the Regional Haze Rule. J. Air Waste Manag. Assoc. 68, 438–445.

Hallar, A.G., Molotch, N.P., Hand, J.L., Livneh, B., McCubbin, I.B., Petersen, R., Michalsky, J., Lowenthal, D., Kunkel, K.E., 2017. Impacts of increasing aridity and wildfires on aerosol loading in the intermountain Western US. Environ. Res. Lett. 12.

Hand, J.L., Malm, W.C., 2007. Review of aerosol mass scattering efficiencies from ground-based measurements since 1990. Journal of Geophysical Research-Atmospheres 112.

Hand, J.L., Ames, R.B., Kreidenweis, S.M., Day, D.E., Malm, W.C., 2000. Estimates of particle hygroscopicity during the southeastern aerosol and visibility study. J. Air Waste Manag. Assoc. 50, 677–685.

Hand, J.L., Kreidenweis, S.M., Kreisberg, N., Hering, S., Stolzenburg, M., Dick, W., McMurry, P.H., 2002. Comparisons of aerosol properties measured by impactors and light scattering from individual particles: refractive index, number and volume concentrations, and size distributions. Atmos. Environ. 36, 1853–1861.

Hand, J.L., Copeland, S.A., Day, D.E., Dillner, A.M., Indresand, H., Malm, W.C., McDade, C.E., Moore, C.T.J., Pitchford, M.L., Schichtel, B.A., Watson, J.G., 2011. IMPROVE (Interagency Monitoring of Protected Visual Environments): spatial and seasonal patterns and temporal variability of haze and its constituents in the United States. http://vista.cira.colostate.edu/Improve/spatial-and-seasonal-patterns-and-temporal-variability-of-haze-and-its-constituents-in-the-united-states-report-v-june-2011/ 507.

Hand, J.L., Schichtel, B.A., Malm, W.C., Pitchford, M.L., 2012. Particulate sulfate ion concentration and SO2 emission trends in the United States from the early 1990s through 2010. Atmos. Chem. Phys. 12, 10353–10365.

Hand, J.L., Schichtel, B.A., Malm, W.C., Copeland, S., Molenar, J.V., Frank, N., Pitchford, M., 2014. Widespread reductions in haze across the United States from the early 1990s through 2011. Atmos. Environ. 94, 671–679.

Hand, J.L., Prenni, A.J., Schichtel, B.A., Malm, W.C., Chow, J.C., 2019. Trends in remote PM2.5 residual mass across the United States: implications for aerosol mass reconstruction in the IMPROVE network. Atmos. Environ. 203, 141–152.

Heald, C.L., Kroll, J.H., Jimenez, J.L., Docherty, K.S., DeCarlo, P.F., Aiken, A.C., Chen, Q., Martin, S.T., Farmer, D.K., Artaxo, P., 2010. A simplified description of the evolution of organic aerosol composition in the atmosphere. Geophys. Res. Lett. 37.

Hidy, G.M., Blanchard, C.L., Baumann, K., Edgerton, E., Tanenbaum, S., Shaw, S., Knipping, E., Tombach, I., Jansen, J., Walters, J., 2014. Chemical climatology of the southeastern United States, 1999-2013. Atmos. Chem. Phys. 14, 11893–11914.

Hyslop, N.P., Trzepla, K., White, W.H., 2015. Assessing the suitability of historical PM2.5 element measurements for trend analysis. Environ. Sci. Technol. 49, 9247–9255.

Jimenez, J.L., Canagaratna, M.R., Donahue, N.M., Prevot, A.S.H., Zhang, Q., Kroll, J.H., DeCarlo, P.F., Allan, J.D., Coe, H., Ng, N.L., Aiken, A.C., Docherty, K.S., Ulbrich, I.M., Grieshop, A.P., Robinson, A.L., Duplissy, J., Smith, J.D., Wilson, K.R., Lanz, V.A., Hueglin, C., Sun, Y.L., Tian, J., Laaksonen, A., Raatikainen, T., Rautiainen, J., Vaattovaara, P., Ehn, M., Kulmala, M., Tomlinson, J.M., Collins, D.R., Cubison, M.J., Dunlea, E.J., Huffman, J.A., Onasch, T.B., Alfarra, M.R., Williams, P.I., Bower, K., Kondo, Y., Schneider, J., Drewnick, F., Borrmann, S., Weimer, S., Demerjian, K., Salcedo, D., Cottrell, L., Griffin, R., Takami, A., Miyoshi, T., Hatakeyama, S., Shimono, A., Sun, J.Y., Zhang, Y.M., Dzepina, K., Kimmel, J.R., Sueper, D., Jayne, J.T., Herndon, S.C., Trimborn, A.M., Williams, L.R., Wood, E.C., Middlebrook, A.M., Kolb, C.E., Baltensperger, U., Worsnop, D.R., 2009. Evolution of organic aerosols in the atmosphere. Science 326, 1525–1529.

Keller, C.A., Long, M.S., Yantosca, R.M., Da Silva, A.M., Pawson, S., Jacob, D.J., 2014. HEMCO v1.0: a versatile, ESMF-compliant component for calculating emissions in atmospheric models. Geosci. Model Dev. (GMD) 7, 1409–1417.

Lee, T., Yu, X.Y., Kreidenweis, S.M., Malm, W.C., Collett, J.L., 2008. Semi-continuous measurement of PM2.5 ionic composition at several rural locations in the United States. Atmos. Environ. 42, 6655–6669.

Liu, J., Russell, L.M., Lee, A.K.Y., McKinney, K.A., Surratt, J.D., Ziemann, P.J., 2017. Observational evidence for pollution-influenced selective uptake contributing to biogenic secondary organic aerosols in the southeastern US. Geophys. Res. Lett. 44, 8056–8064.

Liu, J., Russell, L.M., Ruggeri, G., Takahama, S., Claflin, M.S., Ziemann, P.J., Pye, H.O.T., Murphy, B.N., Xu, L., Ng, N.L., McKinney, K.A., Budisulistiorini, S.H., Bertram, T.H., Nenes, A., Surratt, J.D., 2018. Regional similarities and nox-related increases in biogenic secondary organic aerosol in summertime southeastern United States. Journal of Geophysical Research-Atmospheres 123, 10620–10636.

Lowenthal, D.H., Kumar, N., 2003. PM2.5 mass and light extinction reconstruction in IMPROVE. J. Air Waste Manag. Assoc. 53, 1109–1120.

Lowenthal, D.H., Kumar, N., 2004. Variation of mass scattering efficiencies in IMPROVE. J. Air Waste Manag. Assoc. 54, 926–934.

Lowenthal, D., Zielinska, B., Mason, B., Samy, S., Samburova, V., Collins, D., Spencer, C., Taylor, N., Allen, J., Kumar, N., 2009. Aerosol characterization studies at Great Smoky Mountains national park, summer 2006. Journal of Geophysical Research-Atmospheres 114.

Lowenthal, D., Zielinska, B., Samburova, V., Collins, D., Taylor, N., Kumar, N., 2015. Evaluation of assumptions for estimating chemical light extinction at US national parks. J. Air Waste Manag. Assoc. 65, 249–260.

Luo, G., Yu, F., 2011a. Sensitivity of global cloud condensation nuclei concentrations to primary sulfate emission parameterizations. Atmos. Chem. Phys. 11, 1949–1959.

Luo, G., Yu, F., 2011b. Simulation of particle formation and number concentration over the Eastern United States with the WRF-Chem plus APM model. Atmos. Chem. Phys. 11, 11521–11533.

Luo, G., Yu, F., Schwab, J.J., 2019. Revised Treatment of Wet Scavenging Processes Dramatically Improves GEOS-Chem 12.0.0 Simulations of Nitric Acid, Nitrate, and Ammonium over the United States. Geoscientific Model Development submitted.

Malm, W.C., Day, D.E., 2001. Estimates of aerosol species scattering characteristics as a function of relative humidity. Atmos. Environ. 35, 2845–2860.

Malm, W.C., Hand, J.L., 2007. An examination of the physical and optical properties of aerosols collected in the IMPROVE program. Atmos. Environ. 41, 3407–3427.

Malm, W.C., Sisler, J.F., Huffman, D., Eldred, R.A., Cahill, T.A., 1994. Spatial and seasonal trends in particle concentrationand optical extinction in the United States. Journal of Geophysical Research-Atmospheres 99, 1347–1370.

Malm, W.C., Day, D.E., Kreidenweis, S.M., Collett, J.L., Lee, T., 2003. Humidity-dependent optical properties of fine particles during the Big Bend regional aerosol and visibility observational study. Journal of Geophysical Research-Atmospheres 108.
Malm, W.C., Day, D.E., Carrico, C., Kreidenweis, S.M., Collett, J.L., McMeeking, G., Lee, T., Carrillo, J., Schichtel, B., 2005. Intercomparison and closure calculations using measurements of aerosol species and optical properties during the Yosemite Aerosol Characterization Study. Journal of Geophysical Research-Atmospheres 110.
Malm, W.C., Schichtel, B.A., Pitchford, M.L., 2011. Uncertainties in PM2.5 gravimetric and speciation measurements and what we can learn from them. J. Air Waste Manag. Assoc. 61, 1131–1149.
Malm, W.C., Schichtel, B.A., Hand, J.L., Collett, J.L., 2017. Concurrent temporal and spatial trends in sulfate and organic mass concentrations measured in the IMPROVE monitoring program. Journal of Geophysical Research-Atmospheres 122, 10341–10355.
McClure, C.D., Jaffe, D.A., 2018. US particulate matter air quality improves except in wildfire-prone areas. Proc. Natl. Acad. Sci. U. S. A 115, 7901–7906.
Molenar, J.V., Persha, G., 2008. Optec NGN-2 LED ambient integrating nephelometer. In: AWMA Visibility Specialty Conference, Moab, UT, pp. 5 Extended Abstract #77.
Pitchford, M., Malm, W., Schichtel, B., Kumar, N., Lowenthal, D., Hand, J., 2007. Revised algorithm for estimating light extinction from IMPROVE particle speciation data. J. Air Waste Manag. Assoc. 57, 1326–1336.
Polidori, A., Turpin, B.J., Davidson, C.I., Rodenburg, L.A., Maimone, F., 2008. Organic PM2.5: fractionation by polarity, FTIR spectroscopy, and OM/OC ratio for the Pittsburgh aerosol. Aerosol Sci. Technol. 42, 233–246.
Prenni, A.J., Petters, M.D., Kreidenweis, S.M., DeMott, P.J., Ziemann, P.J., 2007. Cloud droplet activation of secondary organic aerosol. Journal of Geophysical Research-Atmospheres 112.
Prenni, A.J., Day, D.E., Evanoski-Cole, A.R., Sive, B.C., Hecobian, A., Zhou, Y., Gebhart, K.A., Hand, J.L., Sullivan, A.P., Li, Y., Schurman, M.I., Desyaterik, Y., Malm, W.C., Collett, J.L., Schichtel, B.A., 2016. Oil and gas impacts on air quality in federal lands in the Bakken region: an overview of the Bakken Air Quality Study and first results. Atmos. Chem. Phys. 16, 1401–1416.
Ridley, D.A., Heald, C.L., Ridley, K.J., Kroll, J.H., 2018. Causes and consequences of decreasing atmospheric organic aerosol in the United States. Proc. Natl. Acad. Sci. U. S. A 115, 290–295.
Ruthenburg, T.C., Perlin, P.C., Liu, V., McDade, C.E., Dillner, A.M., 2014. Determination of organic matter and organic matter to organic carbon ratios by infrared spectroscopy with application to selected sites in the IMPROVE network. Atmos. Environ. 86, 47–57.
Ryan, P.A., Lowenthal, D., Kumar, N., 2005. Improved light extinction reconstruction in interagency monitoring of protected visual environments. J. Air Waste Manag. Assoc. 55, 1751–1759.
Sickles, J.E., Shadwick, D.S., 2015. Air quality and atmospheric deposition in the eastern US: 20 years of change. Atmos. Chem. Phys. 15, 173–197.
Suda, S.R., Petters, M.D., Yeh, G.K., Strollo, C., Matsunaga, A., Faulhaber, A., Ziemann, P.J., Prenni, A.J., Carrico, C.M., Sullivan, R.C., Kreidenweis, S.M., 2014. Influence of functional groups on organic aerosol cloud condensation nucleus activity. Environ. Sci. Technol. 48, 10182–10190.
Tao, J., Zhang, L.M., Ho, K.F., Zhang, R.J., Lin, Z.J., Zhang, Z.S., Lin, M., Cao, J.J., Liu, S.X., Wang, G.H., 2014. Impact of PM2.5 chemical compositions on aerosol light scattering in Guangzhou - the largest megacity in South China. Atmos. Res. 135, 48–58.
Theil, H., 1950. A rank-invariant method of linear and polynomial regression analysis, I, II and III. In: Proceedings of the Koninklijke Nederlandse Akademie Wetenschappen, Series A – Mathematical Sciences. Statistical Department of the “Mathematisch Centrum”, Amsterdam, the Netherlands, pp. 386–392 521-525, 1357-1412.
U.S.C. § 7475. Preconstruction requirements. Clean Air Act § 165(d).
1 U.S.C. § 7491. Visibility protection for Federal class 1 areas. Clean Air Act § 169A(a)(1).
Valentini, S., Bernardoni, V., Massabo, D., Prati, P., Valli, G., Vecchi, R., 2018. Tailored coefficients in the algorithm to assess reconstructed light extinction at urban sites: a comparison with the IMPROVE revised approach. Atmos. Environ. 172, 168–176.
Weber, R.J., Guo, H.Y., Russell, A.G., Nenes, A., 2016. High aerosol acidity despite declining atmospheric sulfate concentrations over the past 15 years. Nat. Geosci. 9, 282–285.
White, W.H., Trzepla, K., Hyslop, N.P., Schichtel, B.A., 2016. A critical review of filter transmittance measurements for aerosol light absorption, and de novo calibration for a decade of monitoring on PTFE membranes. Aerosol Sci. Technol. 50, 984–1002.
Xu, L., Guo, H.Y., Boyd, C.M., Klein, M., Bougiatioti, A., Cerully, K.M., Hite, J.R., Isaacman-VanWertz, G., Kreisberg, N.M., Knote, C., Olson, K., Koss, A., Goldstein, A.H., Hering, S.V., de Gouw, J., Baumann, K., Lee, S.H., Nenes, A., Weber, R.J., Ng, N.L., 2015. Effects of anthropogenic emissions on aerosol formation from isoprene and monoterpenes in the southeastern United States. Proc. Natl. Acad. Sci. U. S. A 112, 37–42.
Yu, F., Luo, G., 2009. Simulation of particle size distribution with a global aerosol model: contribution of nucleation to aerosol and CCN number concentrations. Atmos. Chem. Phys. 9, 7691–7710.
Yu, L.E., Shulman, M.L., Kopperud, R., Hildemann, L.M., 2005. Fine organic aerosols collected in a humid, rural location (Great Smoky Mountains, Tennessee, USA): chemical and temporal characteristics. Atmos. Environ. 39, 6037–6050.
Yu, F., Luo, G., Ma, X., 2012. Regional and global modeling of aerosol optical properties with a size, composition, and mixing state resolved particle microphysics model. Atmos. Chem. Phys. 12, 5719–5736.
Yu, F., Luo, G., Pryor, S.C., Pillai, P.R., Lee, S.H., Ortega, J., Schwab, J.J., Hallar, A.G., Leaitch, W.R., Aneja, V.P., Smith, J.N., Walker, J.T., Hogrefe, O., Demerjian, K.L., 2015. Spring and summer contrast in new particle formation over nine forest areas in North America. Atmos. Chem. Phys. 15, 13993–14003.
Yu, F., Nadykto, A.B., Herb, J., Luo, G., Nazarenko, K.M., Uvarova, L.A., 2018. H2SO4-H2O-NH3 ternary ion-mediated nucleation (TIMN): kinetic-based model and comparison with CLOUD measurements. Atmos. Chem. Phys. 18, 17451–17474.
Zhang, F., Li, Y., Li, Z., Sun, L., Li, R., Zhao, C., Wang, P., Sun, Y., Liu, X., Li, J., Li, P., Ren, G., Fan, T., 2014. Aerosol hygroscopicity and cloud condensation nuclei activity during the AC(3)Exp campaign: implications for cloud condensation nuclei parameterization. Atmos. Chem. Phys. 14, 13423–13437.
Zhang, F., Li, Z.Q., Li, Y.A., Sun, Y.L., Wang, Z.Z., Li, P., Sun, L., Wang, P.C., Cribb, M., Zhao, C.F., Fan, T.Y., Yang, X., Wang, Q.Q., 2016. Impacts of organic aerosols and its oxidation level on CCN activity from measurement at a suburban site in China. Atmos. Chem. Phys. 16, 5413–5425.
Zheng, C.W., Zhao, C.F., Li, Y.P., Wu, X.L., Zhang, K.Y., Gao, J., Qiao, Q., Ren, Y.Z., Zhang, X., Chai, F.H., 2018. Spatial and temporal distribution of NO2 and SO2 in Inner Mongolia urban agglomeration obtained from satellite remote sensing and ground observations. Atmos. Environ. 188, 50–59.